Received: September 4, 2023. Revised: November 28, 2023. 83

International Journal of
Intelligent Engineering & Systems

http://www.inass.org/

An Ultra-Selective OLR – based Microstrip Diplexer with Minimal Insertion Loss for Wireless Communication System

Rania Hamdy Elabd[1] Ahmed Jamal Abdullah Al-Gburi[2] Khaled Alhassoon[3]
Jamil Abedalrahim Jamil Alsayaydeh[2] Tale Saeidi[4] Naba Jasim Mohammed[5]
Zahriladha Zakaria[2]*

[1]Electronic and Communication Dept., Higher Institute of Engineering and Technology in New Damietta, Damietta 34517, Egypt
[2]Center for Telecommunication Research & Innovation (CeTRI), Fakulti Teknologi dan Kejuruteraan Elektronik dan Komputer (FTKEK), Universiti Teknikal Malaysia Melaka (UTeM), Jalan Hang Tuah Jaya, Durian Tunggal, Melaka 76100, Malaysia
[3]Department of Electrical Engineering, College of Engineering, Qassim University, Unaizah 56452, Saudi Arabia
[4]WiSAR Lab, Atlantic Technological University (ATU), Letterkenny, Co. Donegal F92 FC93, Ireland
[5]Materials Science Program, Department of Applied Physics, Faculty of Science and Technology, University Kebangsaan Malaysia, Bangi 43600, Selangor, Malaysia
* Corresponding author's Email: zahriladha@utem.edu.my

Abstract: This paper presents a high-selectivity, low-insertion-loss open-loop resonator (OLR)-based microstrip diplexer designed for wireless communication systems. We employed a microstrip transmission line with two serial capacitive gaps, incorporating rectangular half-wavelength open-loop resonators, to create a bandpass filter (BPF) with remarkable selectivity. The intended BPFs are interconnected by a T-junction combiner, which is matched to both filters and the antenna port, thereby creating the modelled diplexer. The system is implemented on a Rogers TMM4 substrate featuring a loss tangent of 0.002, a dielectric constant of 4.7, and a thickness of 1.52 mm. The suggested diplexer has dimensions of (90×70) mm². It achieves a modest frequency spacing ratio of R=0.1646 in both transmit and receive modes, with resonance frequencies of f_t = 2.191 GHz and f_r= 2.584 GHz, respectively. The simulated structure demonstrates favorable insertion losses of approximately 1.2 dB and 1.79 dB for the two channels at fractional bandwidths of 1.24% (2.191 GHz) and 0.636% (2.584 GHz). The simulated isolation values at 2.191 GHz and 2.584 GHz are 53.3 dB and 66.5 dB, respectively. Notably, the simulated and measured results exhibit a high degree of consistency. However, minor variations between the simulated and actual results have been noted, primarily attributable to the inherent fabrication tolerances.

Keywords: Microstrip diplexer, Band pass filter (BPF), Open loop resonator (OLR).

1. Introduction

All wireless communication technologies are essential to our daily lives and play a significant part in many wireless system applications [1]. A key component of frequency division duplex technology is the microwave diplexer [2]. Diverse communication technologies, such as radio transmission, mobile telephony, and broadband wireless communications, all depend on diplexers. Matthaei et al. & Wenzel conducted extensive research on diplexers in the 1960s. [3, 4]. These are very discerning parts that can combine or divide signals with various center frequencies.

Devices with three ports that divide an input signal into two channels operating at different frequencies are called diplexers [5] as shown in Fig. 1. There are various methods for creating RF diplexers, but typically three methods are utilized [6]. The first method involves using two band-pass filters with various resonant frequencies. The second

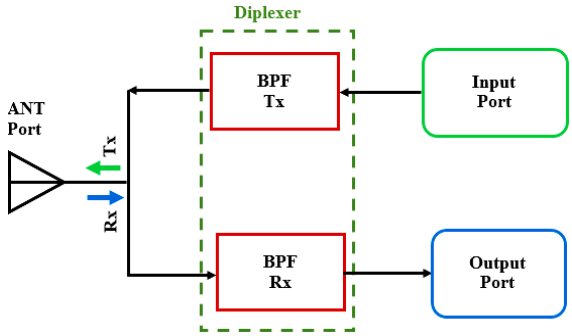

Figure. 1 Diplexer's schematic representation

method uses a band-stop filter to reject the same frequency band for one channel while using a band-pass filter for the other channel. The third method involves using two band-stop filters with different resonant frequencies.

Several types of microstrip diplexers are presented in references [7-23], but the main drawback is that they require a lot of space. Reference [7] proposes a Y-shaped slot antenna with a cavity-backed self-diplexing system using substrate integrated waveguide (SIW) to achieve high isolation. This antenna design has a Y-shaped slot on the top side of the rectangular SIW to produce two asymmetrical radiating apertures for radiation at 3.9 GHz and 4.9 GHz. While this design provides a high-gain antenna, its Tx-Rx isolation of 34 dB is not ideal, and it has a high-frequency space ratio of r=0.227. Reference [8] presents an alternative design, featuring a self-diplexing slot antenna with a bow-tie shape, incorporated within an SIW cavity. This particular design incorporates two separate feed lines to induce resonance within the SIW cavity at both the transmitting and receiving frequencies, yielding a high-gain antenna exhibiting a unidirectional radiation pattern. Nonetheless, it is important to note that this design has a relatively large high-frequency space ratio (r= 0.22) and exhibits limited transmit-receive isolation, measuring at 22 dB.

In reference [9], a microstrip diplexer is employed to merge the global mobile system (GSM) and wireless local area network (WLAN) frequency bands. The negative effects of the microstrip diplexer are reduced by this design. It has some shortcomings, such as significant channel losses and a 30 dB isolation limit. A straightforward method for designing a microstrip diplexer is suggested in [10]. It is built using two small Square OLR band pass filters together. These filters were created for 2.45 GHz Radio Frequency Identification applications. Chebychev's approximation is used. Diplexer isolation is 40 dB.

A dual-mode resonator-based substrate integrated waveguide (SIW) diplexer is suggested in [11]. This diplexer is used to enhance RF front end performance. This diplexer provides appropriate isolation of 49 dB and 53 dB, respectively, for the broadcast and receive channels. Yet, some of its shortcomings are its size.

In reference [12], there is a proposal for the creation of a microstrip diplexer using the design of squared open-loop resonators (SOLRs). This diplexer exhibits a narrow frequency spacing with r = 0.114, and it features two resonance frequencies: 1.81 GHz for the transmit channel and 2.03 GHz for the receive channel. Despite its advantages, the diplexer's dimensions are seen as a drawback., respectively. Despite its benefits, the diplexer's size is considered a limitation.

In reference [13], a dual-band bandpass filter was created by merging two independent channel filters to establish a microstrip diplexer. This approach eliminates the requirement for external junctions during the diplexer's construction, which diverges from conventional techniques that demand separate connections or junctions for distributing energy. Through simulations and experimental observations, the diplexer demonstrated an impressive 50 dB isolation between its transmit and receive bands. Nevertheless, there were discernible insertion losses of 2.88 dB in the transmitting band and 2.95 dB in the receiving band.

In another work referenced as [14], a new shaped microstrip diplexer with improved isolation and selectivity was introduced. This design employs two compact bandpass filters comprised of open/shorted lines and an open stub, tailored for applications related to LTE. For the frequency response performance to be improved, many types of resonators are used [15-20]. Recently, other resonator shapes such as U-shaped [15], Triangular loop resonators [16], T-shaped, [17], have been introduced. Pi-shaped [18], stepped-impedance [19], and Patch resonators [20,21]. Patch resonators are utilized in [22] to produce a filtering response. In order to create a microstrip diplexer, two bandpass filters (BPFs) made of spiral cells and coupled lines are integrated in [23]. It has some drawbacks, including unwanted harmonics and large losses at both channels. The configuration of the showcased microstrip diplexer in reference [24] employs a setup involving three interconnected line structures to enhance the attenuation of harmonics. Nonetheless, the challenge of notable signal losses in both channels persists. On the other hand, the proposed diplexer outlined in reference [25] offers the potential to efficiently mitigate harmonic distortions and also lower the simulated insertion losses for both channels. However, both channels exhibit substantial common port return losses in this arrangement.

Table 1. Detailed comparison of latest technology of microstrip diplexer for wireless communication systems with the existing literature

#	Reference	Size λ_g^2	Frequency (GHz)	FBW (%)	Insertion Loss (dB)	Isolation (dB)	R
1	[9]	0.35	1.8/2.4	6/5.8	NA	30	0.286
2	[10]	1.2	2.2/2.6	4.55/5	1.6/1	40	0.167
3	[11]	4.6	8.04/9.07	4.23/4.19	2.35/2.33	49/53	0.12
4	[12]	1.5	1.81/2.03	2.25/3	1.98/1.9	58/46	0.114
5	[14]	0.167	1.8/2.1	5.5/6.2	2/1.8	40	0.154
6	[22]	0.89	1.85/2.5	NA	4.2/3.3	31	NA
7	[23]	0.98	1.41/2.02	NA	4.4/4.6	29	NA
8	[25]	0.3	1.5/2.1	NA	1.5/1.8	45	NA
9	[26]	3.5	9.5/10.6	6	2.6/2.3	45	NA
This work		0.435	2.191/2.584	1.24/0.636	1.2/1.79	53.3/66.5	0.1646

In contrast to the simulated insertion losses at both channels in [26], which are relatively low, the

introduced diplexer in [27] has substantial losses at both channels. The suggested structure, however, was unable to achieve modest return losses at either its up-per or lower channels.

As endeavors are underway to develop a compact microstrip bandpass diplexer with high-performance

characteristics, the design aspects, such as low losses and increased fractional band-width, make it difficult to sacrifice the compact size.

This work introduces a high isolation and low insertion loss effective design scheme for microstrip diplexers. The two-compact size BPFs that make up the proposed diplexer are constructed from linked OLRs. A T-junction that serves as a combining circuit connects the two BPFs to the antenna and provides good isolation between the up-link and down-link BPFs. Initially, a high selectivity BPF is created for 2.191 GHz operation. The suggested microstrip diplexer is then made up of the other BPF, which is created to operate at 2.584GHz, and the first BPF.

The suggested diplexer exhibits excellent size-related characteristics and performance., resonance frequency (GHz) at transmit channel and receive channel, (FBW (GHz)), insertion loss (dB), isolation (dB), and frequency space ratio (R), compared to #1 up to #9. Table 1 presents a comparative analysis of various diplexer designs, showcasing a competitive version among the options available.

The critical contributions of this paper are listed below:

1) A compact diplexer with high selectivity, fractional bandwidths of 1.24% and 0.636%, low insertion losses of 1.2 dB and 1.79 dB, and a low frequency space ratio of 0.1646 was proposed.
2) A miniaturized two-bandpass filters (BPFs) were obtained, with the first one for the transmit channel and the second for the receive channel. The total physical dimension of the filters was 25 mm x 25 mm x 1.52 mm, with a resonance frequency of 2.191 GHz and 2.584 GHz for the transmit and receive channels, respectively.
3) A diplexer was obtained by assembling the two BPFs in an orthogonal manner through a T-junction to achieve the highest isolation of 53.3 dB and 66.5 dB for the transmit and receive channels, respectively.
4) An LC equivalent circuit and numerical formula were proposed for the BPF and diplexer to comprehend their behavior.

2. Proposed OLR-based microstrip diplexer

Generally, two band pass filters are constructed as the initial step in the microstrip diplexer design process. n this section, an alternative design is introduced for a highly efficient microstrip diplexer

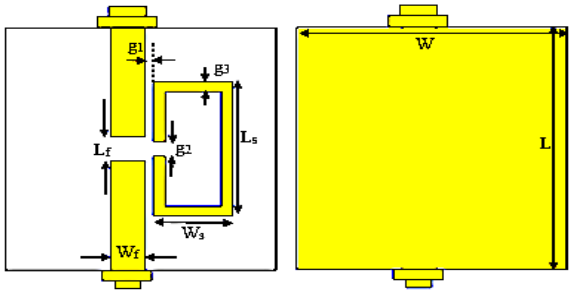

(a) (b)

Figure. 2 The geometrical construction of the OLR- BPF at $f_t = 2.191GHz$ for both: (a) front and (b) back views

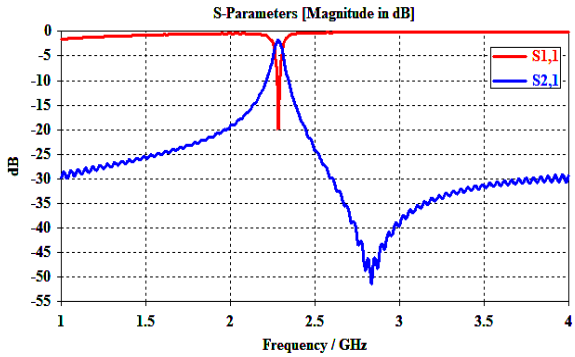

Figure. 3 The receive BPF's simulated S-parameters

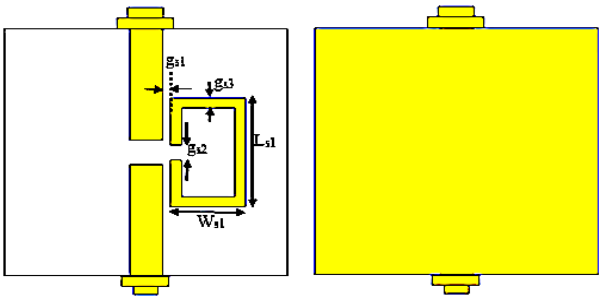

(a) (b)

Figure. 4 The geometrical construction of the OLR-based BPF at $f_t = 2.584\ GHz$ for both: (a) front and (b) back perspectives

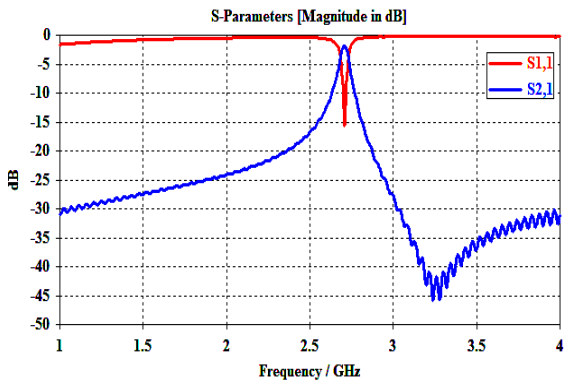

Figure. 5 The transmit BPF's simulated S-parameters

that operates at f_t=2.191 GHz for transmit mode and f_r=2.584 GHz for receive mode, is shown using the computer simulation technology (CST) software.

The Rogers TMM4 substrate, as mentioned earlier, hosts the diplexer design on both of its surfaces. In order to achieve the desired transmit and receive frequencies, f_t= 2.191 GHz and f_r= 2.584 GHz, respectively, two selective BPFs are joined together to form the proposed diplexer. The T-junction is used to join the two BPFs together. As a result, the suggested diplexer's design process can be completed in the following two steps: (i) The transmit and receive BPF designs. (ii) The planned microstrip diplexer's meeting.

2.1 Creation of the transmit and receive bandpass filters (BPFs)

This section describes the designs of the transmit and receive bandpass filters (BPFs). Fig. 2, illustrates the proposed topology for the microstrip BPF, which includes two input/output feed lines and a rectangular open-loop resonator. The interaction between the two transmission lines and the resonator is achieved through gap g_1, with gap L_f serving as the separator between the two feed lines. The incorporation of a folded microstrip resonator, along with strategic positioning of the two feed lines, contributes to the enhanced compactness of this design.

Table 2. The suggested transmit and receive BPF's dimensions

Parameter	Value (mm)	Parameter	Value (mm)
W	25	L_{s1}	11.2
L	25	g_1	0.75
W_f	3.06	g_2	1.5
L_f	2.5	g_3	1
W_s	7	g_{s1}	0.75
L_s	14	g_{s2}	1.75
W_{s1}	7	g_{s3}	1

CST-MWS-2019 was used to investigate the operation of the BPF and simulate the shown OLR-BPF, which are printed on a 1.52mm Rogers TMM4 substrate. At the transmit frequency of f_t= 2.191GHz, OLRs are used, as shown in Figure 2 each with a total length of roughly $\lambda_g/2$. Table 2 contains a list of the filter's dimensions. The width and length of the trace line, coupled with the separation gap g_1, determine each resonator's internal capacitance, which in turn influences the filter's selectivity and insertion loss.

The CST Microwave Studio was used to simulate the scattering parameters for the proposed transmit

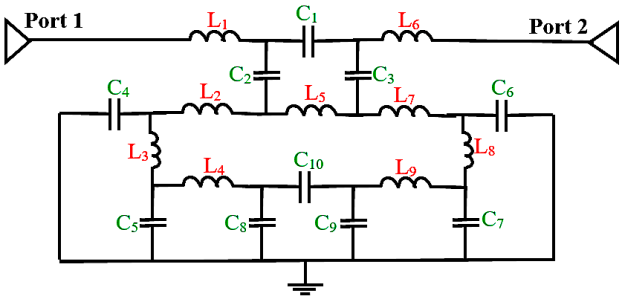

Figure. 6 The proposed BPF's LC equivalent circuit

bandpass filter (BPF), as shown in Fig. 3. This BPF operates at a center frequency of 2.191 GHz and boasts a 3 dB bandwidth spanning 47.1 MHz, with FBR of 1.24%, a return loss of 20 dB, and an insertion loss of 1.4 dB. These parameters align with a range of specified criteria. The suggested receive BPF, which has dimensions indicated in Table 2, is depicted in Fig. 4, and follows the same conceptual framework. Fig. 5, displays the receive BPF's simulated scattering parameters. The curves' analysis reveals the BPF's center frequency to be 2.584 GHz, 3dB bandwidth to be 20.7 MHz, fractional bandwidth to be 0.636%, return loss to be 15.6 dB, and insertion loss to be 1.3 dB.

In the second approach within this study, we focus on analyzing the proposed topology by transforming the microstrip structure into its corresponding LC model, as depicted in Fig. 6. This transformation is carried out with the aim of obtaining a deeper insight into the performance of the suggested BPF.

The proposed topology is symmetric, which enables the use of half circuit LC analysis to convert and transforming the microstrip transmission lines into the LC model, as depicted in Fig. 6. In this LC model, the microstrip transmission lines are assumed to be lossless, while the corresponding LC model is an approximation. The inductances of the central transmission lines are represented by L_1, L_2, L_3, L_4, L_5, L_6, L_7, L_8, and L_9 in this LC model. Within the model, C_1 is utilized to denote the capacitive impact of the space between the two feed-lines. Meanwhile, C_2 and C_3 are assigned to signify the capacitive effects of the gaps between the feed line and the resonator. Furthermore, C_8 and C_9 are attributed to encapsulate the capacitive consequences of the open stubs concerning the ground. Lastly, the capacitive ramifications of the bends are symbolized by C_3, C_4, C_5, and C_6. Every component of the microstrip line is then transformed to an equivalent LC lumps after being divided into smaller sections to assist the conversion process. The electrical parameters of each component are derived using the calculation method detailed in the section below, as referenced in [28]. Lastly, certain tweaking approaches are used to improve the match between the simulation results of the two circuits. The Eqs. (1) and (2) are applied in order to determine the values of each element in the LC configuration.

$$l = CZ_c\, v_p \tag{1}$$

$$l = \frac{Lv_p}{Z_c} \tag{2}$$

If we maintain a consistent line width, we employ the variables C and L to signify the length, capacitance, and inductance of a microstrip line. The characteristic impedance is indicated as Z_c, and the phase velocity is denoted as v_p.

Z_c and v_p must first be determined in order to calculate the C and L values. When the effective dielectric constant ε_{re} has been established, the phase velocity is derived by:

$$v_p = \frac{c}{\varepsilon_{re}} \tag{3}$$

The symbol c presents the speed of light in a vacuum. The equations below can be utilized to determine the characteristic impedance Z_c and effective dielectric constant ε_{re}:

For $W_f/h \leq 1$

$$\varepsilon_{re} = \frac{\varepsilon_r+1}{2} + \frac{\varepsilon_r-1}{2}\left\{\left(1+12\frac{h}{W_f}\right)^{-0.5}\right\} + 0.04\left(1-\frac{W_f}{h}\right)^2 \tag{4}$$

$$Z_c = \frac{\eta}{2\pi\sqrt{\varepsilon_{re}}} ln\left[8\frac{h}{W_f} + 0.25\frac{W_f}{h}\right] \tag{5}$$

For $W_f/h \geq 1$

$$\varepsilon_{re} = \frac{\varepsilon_r+1}{2} + \frac{\varepsilon_r-1}{2}\left(1+12\frac{h}{W_f}\right)^{-0.5} \tag{6}$$

$$Z_c = \frac{\eta}{\sqrt{\varepsilon_{re}}}\left[\frac{h}{W_f} + 1.393 + 0.677\, ln\left\{\frac{W_f}{h} + 1.444\right\}\right]^{-1} \tag{7}$$

Where W_f is the microstrip line's width, h and ε_r are the substrate's thickness and permittivity, ε_{re} is its effective permittivity, and the value $\eta = 120\pi\Omega$ symbolizes the characteristic impedance in a vacuum. Each right-angle bend within the microstrip open-loop resonator can be modelled using an analogous T-network configuration, as illustrated in reference [29]. The formulas (8) and (9) provide a roughly form

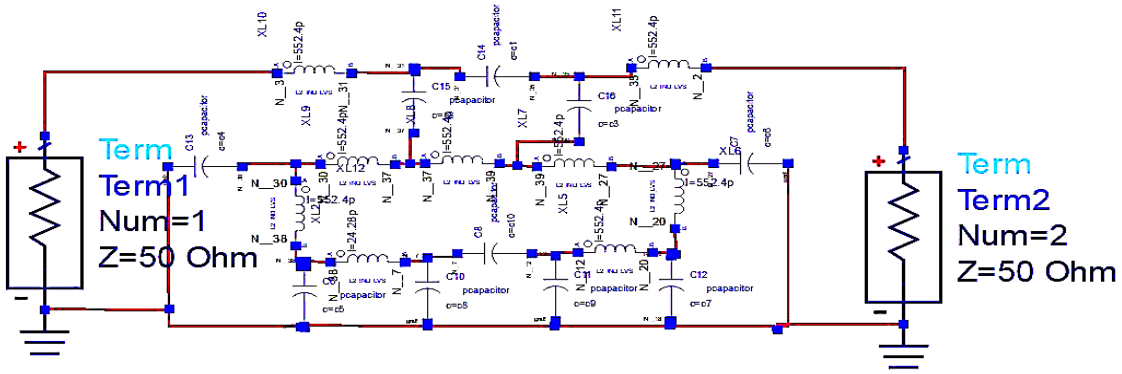

Figure. 7 The schematic circuit model of the proposed BPF in ADS simulation program

for calculating the capacitance in this work.

$$\frac{C}{W_f}(PF/m) = \frac{(14\varepsilon_r+12.5)W_f/h-(1.83\varepsilon_r-2.25)}{\sqrt{W_f/h}} + \frac{0.02\varepsilon_r}{W_f/h} \; for \; W_f/h < 1 \quad (8)$$

$$\frac{C}{W_f}(PF/m) = (9.5\varepsilon_r + 1.25)\, W_f/h + 5.2\varepsilon_r + 7 \text{ for } W_f/h > 1 \quad (9)$$

The effective dielectric constant and the characteristic impedance are the two primary parameters that should be determined, therefore for a line width $W_f = 3.06mm$, we obtain ($\varepsilon_{re} = 3.55$, $Z_c = 49.9$). The modified circuit is then simulated in a schematic environment, following the use of the calculating procedure.

Several simulations were conducted, adjusting the values of each variable in the LC lumps to achieve a closer alignment between the electromagnetic (EM) simulation outcomes and the converted circuit results. The LC-based equivalent circuit of the suggested bandpass filter (BPF) underwent simulation using the ADS electromagnetic simulator.

The proposed BPF's schematic circuit model is shown in Fig. 7, using the ADS simulation tool. The simulated scattering parameters of the LC model using ADS are shown in Fig. 8. It is noticed that the behavior of the BPFs is ideal and allows to pass frequency 2.191GHz for transmit channel as shown in Fig. 8(a), at values of the LC components as follow:

$L_1 = 0.01.$, $L_2 = 0.01.$, $L_3 = 0.01.$, $L_4 = 0.01.$, $L_5 = 0.01.$, $L_6 = 0.01.$, $L_7 = 0.009.$, $L_8 = 0.01.$, $L_9 = 0.01.$ (all in nH). $C_1 = 4.8.$, $C_2 = 1e-6.$, $C_3 = 0.17$, $C_4 = 1e-6.$, $C_5 = 1e-6$, $C_6 = 8.6$, $C_7 = 1.4$, $C_8 = 7.4$, $C_9 = 6$, $C_{10} = 0.12$ (all in pF).

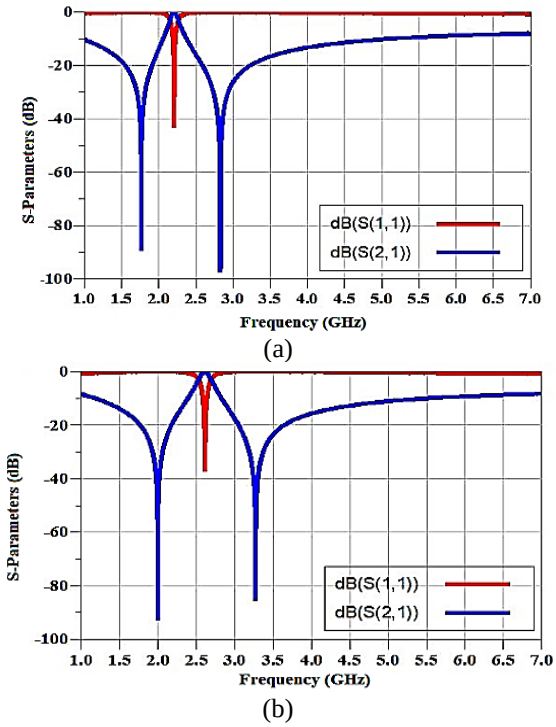

Figure. 8 Scattering parameter of proposed BPF equivalent circuit in ADS simulation program: (a) At 2.191GHz, and (b) At 2.584GHz

Variation of some of the proposed structure's geometric characteristics is one of the key researches to comprehend the behaviour of the suggested band pass filter. This represents an intriguing method to enhance the filter's performance. It was discovered that a crucial design element was the distance L_f between the two feed lines. Many simulations were completed in this context to explore the frequency responses of the filter at various gap L_f values.

The results from the simulation of the S_{21}

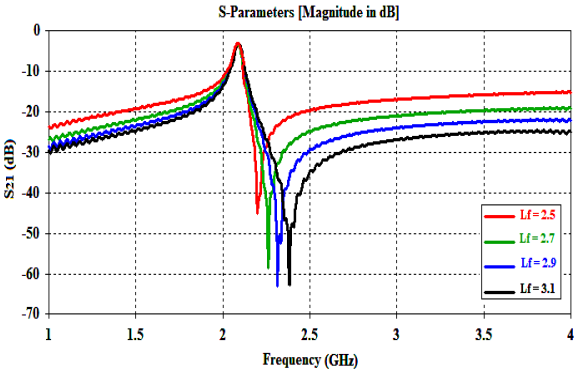

Figure. 9 The simulated S21 parameter at various gap L_f value

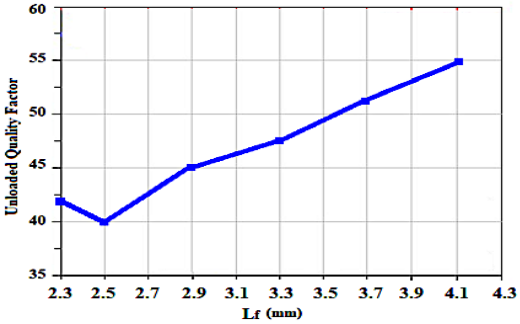

Figure. 10 The progression of the quality factor without a load in the simulation as it varies with different values of gap L_f

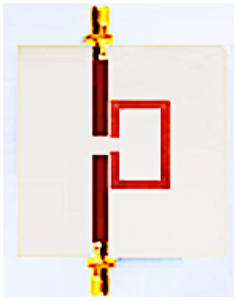

Figure. 11 Manufactured prototype of the suggested BPF

parameter for various space sizes are presented in Fig. 9. The figure reveals two notable outcomes. The first consequence pertains to the bandwidth, where an increase in gap width causes a slight increase in insertion losses and a reduction in bandwidth due to a smaller area between the feed lines and the resonator's periphery. Meanwhile, changing the gap width can impact the position and weakening of the transmission zero, as shown in the figure. The position and weakening of the transmission zero increase as the gap width widens, indicating enhanced selectivity. The existence of the transmission zero results from the cross-coupling between the two resonator arms and the two input/output lines. Hence, modifying the space size can account for the observed behaviour.

Modifying the gap size also impacts the return

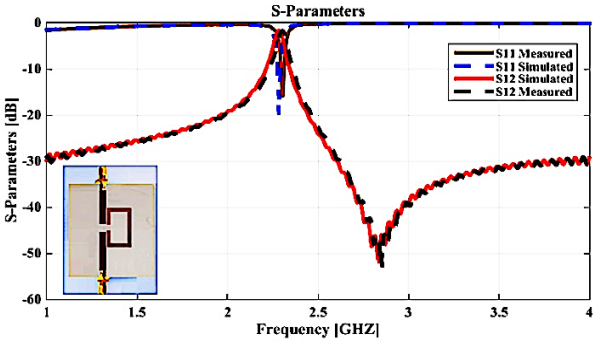

Figure. 12 Evaluating the scattering parameters of the designed bandpass filter (BPF) through a comparison of measured and simulated results

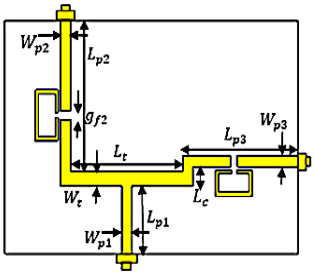

(a)

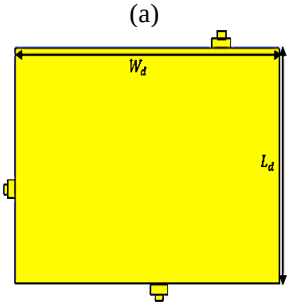

(b)

Figure. 13 The suggested diplexer's construction: (a) top view, and (b) Bottom view

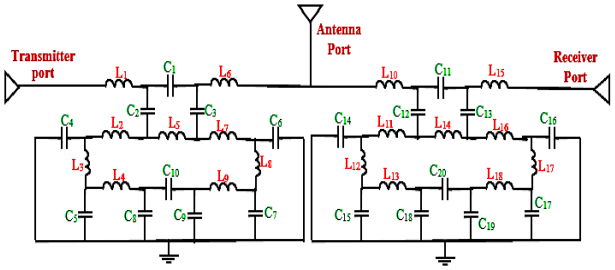

Figure. 14 The proposed BPF's LC equivalent circuit

loss of the filter. The band pass filter's unloaded quality factor Q_o, which can be calculated using Eq. (11), can serve as an indicator of its electrical performance and provide a better understanding of the band pass filter's insertion loss and selectivity, according to reference [30].

$$Q_L = \frac{1}{\frac{2}{Q_e}+\frac{1}{Q_0}} = \frac{f_0}{(\Delta f)_{3dB}} \quad (10)$$

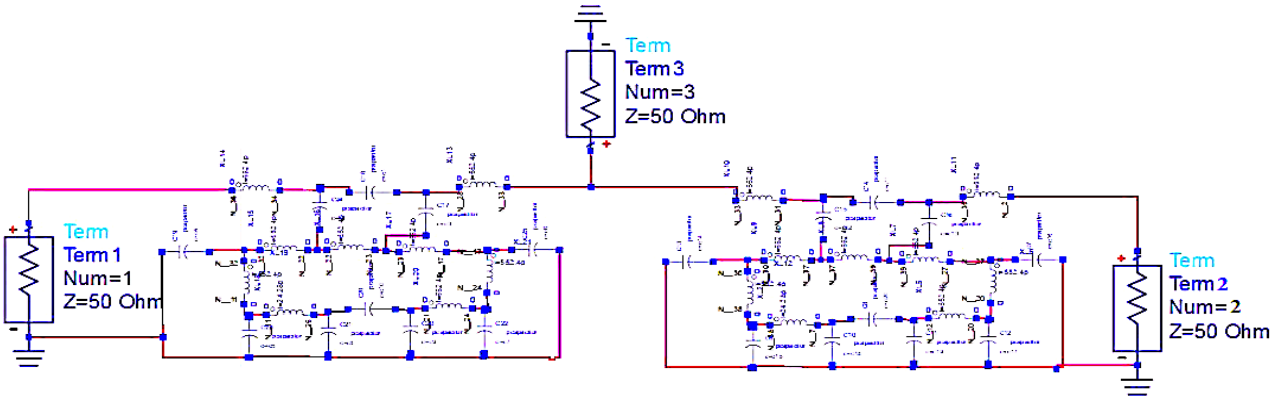

Figure. 15 The schematic circuit model of the proposed diplexer in ADS simulation program

Table 3. The suggested diplexer's dimensions

Parameter	Value (mm)	Parameter	Value (mm)
W_d	90	W_{p2}	3.065
L_d	70	L_{p2}	41.2
W_{p1}	3.056	W_{p3}	3.065
L_{p1}	25	L_{p3}	32
W_t	405	g_{f2}	2.5
L_t	33.9	L_c	5.4

$$Q_0 = \frac{Q_L}{(1-10^{-IL/20})} \quad (11)$$

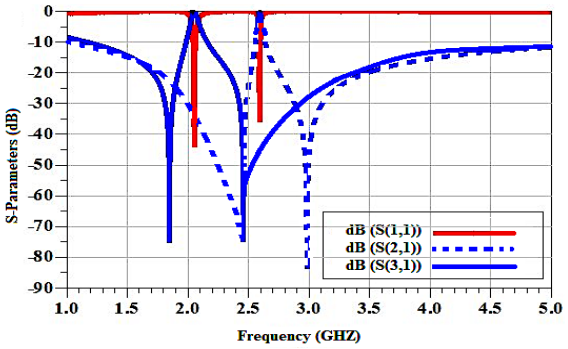

Figure. 16 Simulated scattering parameters of the LC equivalent circuit

With Q_L being the loaded Q determined by the equation, where f_0 is the resonant frequency and $(\Delta f)_{3dB}$ is the pass band's - 3 dB bandwidth (10). Q_e is an indicator of external quality.

The illustration in Fig. 10, demonstrates that the quality factor without any load increases as the separation between the two feed lines is widened. Expanding the space width from 2.3 mm to 4.1 mm results in larger filter dimensions, which in turn contribute to increased radiation loss and reduced conduction loss. This shift in current density, which is associated with the elevated quality factor without load, can be attributed to these observations, as noted in reference [30]. Fig. 11, depicts the proposed BPF as a fabricated prototype on a Rogers TMM4 substrate with dimensions of $(25 \times 25)\, mm^2$. Fig. 12, illustrates a side-by-side evaluation of the measured and simulated S-parameters $|S_{11}|$, and $|S_{21}|$ for the suggested BPF, employing the VNA spectrum. The simulation results closely aligned with the measurements, demonstrating a strong level of agreement.

2.2 The suggested microstrip diplexer's assembly

The two OLR-based BPFs discussed before and discussed in Sec. 2.1 are connected by a T-junction in this section to introduce the whole structure of the suggested diplexer as presented in Fig. 13. The isolation among transmit and receive channels is controlled by the width and length of the T-junction branches. Table 3 has a list of the proposed diplexer's dimensions.

A second method to studying this topology by converting the microstrip diplexer to its corresponding LC model, as shown in Fig. 14, in order to comprehend the behaviour of the suggested diplexer.

Within this LC representation, the characteristics $L_{1.}$, $L_{2.}$, $L_{3.}$, $L_{4.}$, $L_{5.}$, $L_{6.}$, $L_{7.}$, $L_{8.}$, $L_{9.}$, $C_{1.}$, $C_{2.}$, $C_{3.}$, $C_{4.}$, $C_{5.}$, $C_{6.}$, $C_{7.}$, $C_{8.}$, $C_{9.}$, C_{10} represent the transmitter BPF and $L_{10.}$, $L_{11.}$, $L_{12.}$, $L_{13.}$, $L_{14.}$, $L_{15.}$, $L_{16.}$, $L_{17.}$, $L_{18.}$, $C_{11.}$, $C_{12.}$, $C_{13.}$, $C_{14.}$, $C_{15.}$, $C_{16.}$, $C_{17.}$, $C_{18.}$, $C_{19.}$, and C_{20} represent the Reciever BPF, the two filters grouped together with T junction. Fig. 15, represents the Schematic circuit model of the proposed diplexer in ADS simulation program, and Fig. 16, represents the simulated scattering parameters of the LC equivalent circuit. It is noticed that the behaviour of the diplexer is ideal and allows to pass frequencies 2.191GHz and 2.584 GHz at specified value of L and C as follow: $C_1 = 0.18.$, $C_2 = 0.16.$, $C_3 = 7.8.$, $C_4 = 0.12.$, $C_5 = 0.3.$, $C_6 = 0.11.$, $C_7 = 9.0$, $C_8 = 0.1.$, $C_9 = 0.14.$, $C_{10} = 0.136.$, $C_{11} = 0.2.$, $C_{12} = 9.8.$, $C_{13} = 3.2.$, $C_{14} = 0.15.$, $C_{15} = 7.2.$, $C_{16} = 8.6.$, $C_{17} = 9.2.$, $C_{18} = 7.4.$, $C_{19} = 0.174.$, $C_{20} = 0.118.$ (all in PF), $L_1 = 0.01.$, $L_2 = 0.01.$, $L_3 = 0.01.$,

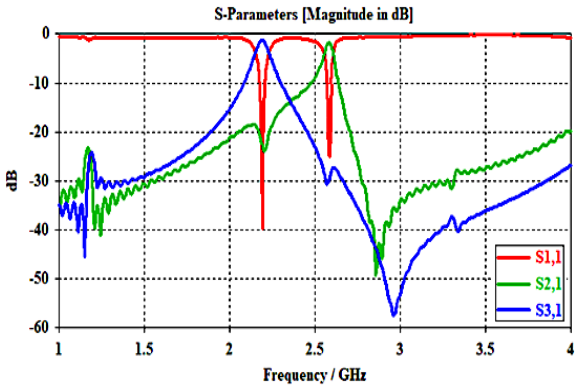

Figure. 17 The suggested diplexer's simulated S-parameters

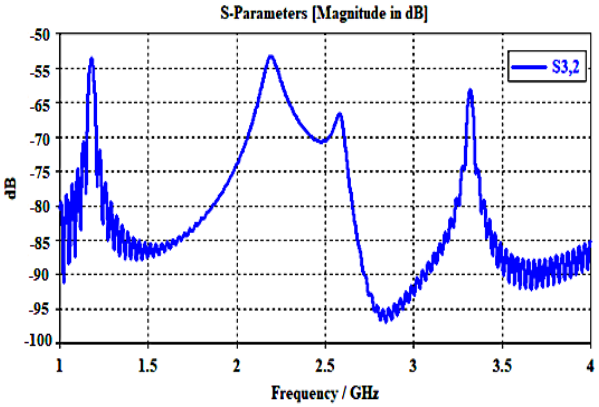

Figure. 18 The suggested diplexer's simulated scattering parameter$|S_{32}|$

$L_4 = 0.01.$, $L_5 = 0.01.$, $L_6 = 0.01.$, $L_7 = 0.009.$, $L_8 = 0.01.$, $L_9 = 0.01.$, $L_{10} = 0.01.$, $L_{11} = 0.01.$, $L_{12} = 0.01.$, $L_{13} = 0.01.$, $L_{14} = 0.01.$, $L_{15} = 0.01.$, $L_{16} = 0.009.$, $L_{17} = 0.01.$, $L_{18} = 0.01.$ (all in nH).

Fig. 17, displays the simulation results of the proposed diplexer's scattering parameters $|S_{11}|$,$|S_{21}|$, and $|S_{31}|$ versus frequency. For the transmit and receive channels, respectively, the structure displays good insertion losses of around 1.2 dB and 1.7 dB, with fractional bandwidths of 1.24% at $f_t = 2.191\ GHz$ and 0.636% at $f_r = 2.584\ GHz$. To put it another way, the transmit and receive bands' respective 3dB bandwidths are 36 MHz and 21.1 MHz, and the corresponding simulated return losses are 40 dB and 26 dB. The scattering parameter $|S_{32}|$ is displayed in Fig. 18. The simulated isolation levels stand at 53.3 dB for 2.191 GHz and 66.5 dB for 2.584 GHz, respectively.

Additionally, the suggested diplexer achieves a modest frequency spacing ratio, denoted as R, equal to 0.1646. This measure is delineated as the difference between the transmit and receive frequencies $\Delta f = |f_r - f_t|$ in relation to the central frequency $f_c = (f_t + f_r)/2$ with R expressed as per the definition in reference [31].

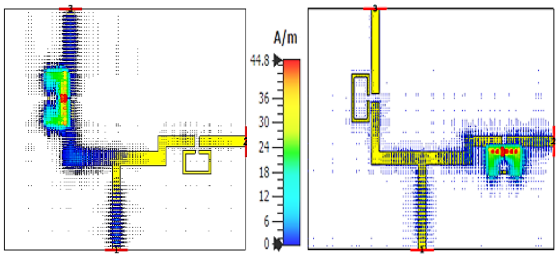

Figure. 19 Distribution of surface current in the suggested diplexer at: (a) $f_t = 2.191\ GHz$, and (b) $f_r = 2.584\ GHz$

$$R = \frac{\Delta f}{f_c} \tag{12}$$

Fig. 19, showcases the computed current distributions of the proposed diplexer at both the transmit and receive frequencies. When the diplexer is configured for transmission at f_t=2.191 GHz, as seen in Fig. 19(a), there is a substantial current density along the path connecting port 1 to port 3, while the pathway from port 1 to port 2 remains inactive. In contrast, when the diplexer operates at the receive frequency f_t=2.584 GHz, as depicted in Figure 19(b), the route from port 1 to port 2 exhibits significant current density, while the connection from port 1 to port 3 remains inactive. As a result, effective isolation is achieved between the broadcasting and receiving channels.

3. Constructed prototype of the suggested diplexer

The modelled diplexer, illustrated in Fig. 20, has been fabricated and printed on a Rogers TMM4 substrate with dimensions of $(90 \times 70)\ mm^2$. The diplexer's performance was evaluated by measuring its S-parameters, namely $|S_{11}|$, $|S_{21}|$, and $|S_{31}|$, using a Vector Network Analyzer (VNA) model Rohde & Schwarz ZVL20, as well as through simulations, as depicted in Fig. 21. The scattering parameter $|S_{32}|$ of the diplexer was also compared between measurements and simulations in Fig. 22. Although there were slight differences in the frequency, the error percentage $\frac{f_{measured} - f_{simulated}}{f_{measured}}$ did not exceed 5%.

4. Conclusion

The focus of this paper is on the development of a microstrip diplexer that utilizes OLR BPFs for wireless communication systems. The diplexer is engineered to attain excellent selectivity, robust isolation, minimal frequency spacing, and low

(a) (b) (c)

Figure. 20 Made-up model of the planned diplexer: (a) Overhead perspective, (b) Underneath perspective, and (c) Experimental arrangement

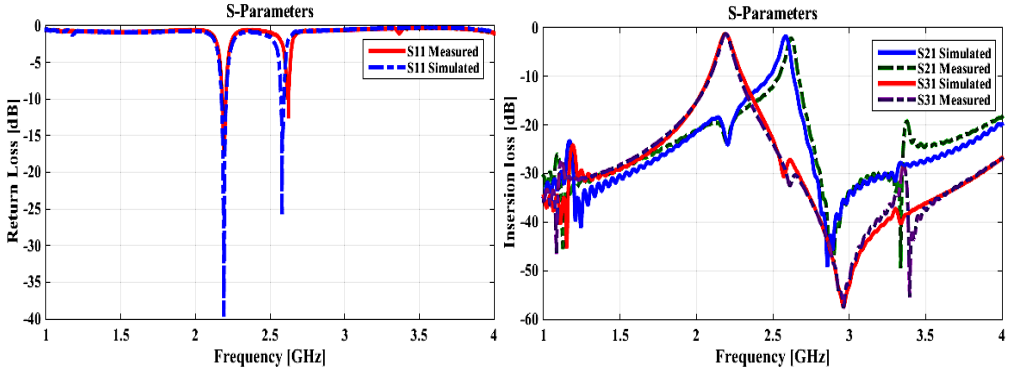

(a) (b)

Figure. 21 The suggested diplexer's measured and simulated scattering parameters: (a) $|S_{11}|$ and (b) $|S_{21}|$, and $|S_{31}|$

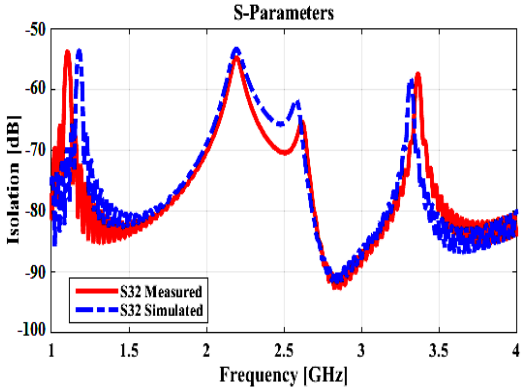

Figure. 22 The suggested diplexer's measured and simulated scattering parameter$|S_{32}|$

insertion loss. It functions within the frequency range of ft=2.191 GHz and f_r=2.584 GHz, employing the Roger TMM4 substrate known for its low electrical loss and stable dielectric constant across the frequency spectrum. The suggested diplexer design has been subjected to simulation using CST software, and the results demonstrate excellent performance with high isolation of approximately 53.3 dB and 66.5 dB for 2.191 GHz and 2.584 GHz, respectively. It also demonstrates the lowest insertion loss of approximately 1.2 dB for the transmit channel and 1.7 dB for the receive channel, as well as an acceptable frequency space ratio of approximately 0.1646 and small fractional bandwidths of 1.24% and 0.636% for the transmit and receive channels, respectively. The performance of the manufactured diplexer was assessed, and a numerical equation for the LC equivalent circuit of the recommended BPF and the suggested microstrip diplexer was built. The finalized diplexer is well suited for wireless communication systems due to its miniaturized size, minimal insertion loss, and great selectivity.

Acknowledgments

The authors would like to thank and acknowledge the support from Universiti Teknikal Malaysia Melaka (UTeM) and the Ministry of Higher Education of Malaysia (MOHE).

Conflicts of interest

The authors declare no conflict of interest.

Author contributions

Conceptualization, Rania Hamdy Elabd, Ahmed Jamal Abdullah Al-Gburi and Zahriladha Zakaria; methodology, Rania Hamdy Elabd; software, Ahmed Jamal Abdullah Al-Gburi; validation, Jamil Abedalrahim Jamil Alsayaydeh, Tale Saeidi, and Naba Jasim Mohammad; formal analysis, Jamil

Abedalrahim Jamil Alsayaydeh; investigation, Ahmed Jamal Abdullah Al-Gburi; resources, Rania Hamdy Elabd; data curation, Rania Hamdy Elabd; writing—original draft preparation, Rania Hamdy Elabd; writing—review and editing, Ahmed Jamal Abdullah Al-Gburi and Khaled Alhassoon; visualization, Naba Jasim Mohammad and Khaled Alhassoon; supervision, Ahmed Jamal Abdullah Al-Gburi; project administration, Ahmed Jamal Abdullah Al-Gburi; funding acquisition, Ahmed Jamal Abdullah Al-Gburi. All authors have read and approved the final manuscript.

References

[1] Z. Jiayu, Q. Deli, and Q. Haifeng, "Virtual full-duplex buffer-aided relay selection schemes for secure cooperative wireless networks", *J Wireless Com Network*, Vol. 44, 2022.

[2] L. Zhou, W. Zhou, Y. Sun, Y. Han, J. Jiang, and D. Zhang, "Design of High-Order Resonator HTS Diplexer with Very Different FBW", *Electronics*, Vol. 12, No. 69, 2023.

[3] G. L. Matthaei and E. G. Cristal, "Multiplexer channel-separating units using interdigital and parallel-coupled filters", *Microwave Theory and Techniques- IEEE Transactions on Microwave Theory and Techniques*, Vol. 13, No. 3, pp. 328-334, 1965.

[4] R. J. Wenzel, "Printed-circuit complementary filters for narrow bandwidth multiplexers", *Microwave Theory and Techniques. IEEE Transactions on Microwave Theory and Techniques*, Vol. 16, No. 3, pp. 147–157, 1968.

[5] S. Roshani, S. I. Yahya, Y. S. Mezaal, M. A. Chaudhary, A. A. A. Hilali, A. Mojirleilani, and S. Roshani, "Design of a Compact Quad-Channel Microstrip Diplexer for L and S Band Applications", *Micromachines*, Vol. 14, p. 553, 2023, doi: 10.3390/mi14030553.

[6] C. G. Abdessamed, "Review on technologies used to design RF diplexers", *Int J Biosen Bioelectron*, Vol. 4, No. 1, pp. 23–25, 2018.

[7] A. A. Ayman, "Design of highly compact self-diplexing Y-shapedslot antenna employing quarter-mode substrate integrated waveguide", *Int J RF Microw Comput Aided Eng*, Vol. 31, 2021. DOI: 10.1002/mmce.22827.

[8] S. Mukherjee and A. Biswas, "Design of self-diplexing substrate integrated waveguide cavity backed slot antenna", *IEEE Antennas and Wireless Propagation Letters*, Vol. 15, pp. 1775–1778, 2016.

[9] W. Feng, X. Gao, and W. Che, "Microstrip diplexer for GSM and WLAN bands using common shorted stubs", *Electronics Letters*, Vol. 50, pp. 1486–1488, 2014. DOI: 10.1049/el.2014.2500.

[10] H. Tizya, F. Riouch, and, A. Tribak, "Microstrip diplexer design based on two square open loop bandpass filters for RFID applications", *International Journal of Microwave and Wireless Technologies*, Vol. 10, No. 4, pp. 412–421, 2018. DOI: 10.1017/S1759078718000314.

[11] F. Cheng, C. Gu, and B. Zhang, "High isolation substrate integrated waveguide diplexer with flexible transmission zeros", *IEEE Microwave and Wireless Components Letters*, Vol. 30, No. 11, pp. 1029–1032, 2020.

[12] M. M. Shaheen, N. M. Mahmoud, A. Alim, M. E. Nasr, and A. H. Hussien, "Implementation of a Highly Selective Microstrip Diplexer with Low Insertion Loss Using Square Open-Loop Resonators and a T-Junction Combiner", *Radio Engineering*, Vol. 31, 2022.

[13] A. O. Nwajana and K. S. K. Yeo, "Microwave diplexer purely based on direct synchronous and asynchronous coupling", *Radio Engineering*, Vol. 25, pp. 247–252, 2016, doi: 10.13164/re.2016.0247.

[14] W. Feng, M. Hong, and W. Che, "Microstrip diplexer design using open/shorted coupled lines", *Progress In Electromagnetics Research Letters*, Vol. 59, pp. 123–127, 2016, doi: 10.2528/PIERL16030805.

[15] G. Karimi, A. Lalbakhsh, K. Dehghani, and H. Siahkamari, "Analysis of novel approach to design of ultra-wide stopband microstrip low-pass filter using modified u-shaped resonator", *ETRI J*., Vol. 37, pp. 945–950, 2015.

[16] S. Roshani, “Design of a Compact Quad-Channel Microstrip Diplexer for L and S Band Applications”, *Micromachines*, Vol. 14, No. 3, p. 553, 2023, doi: 10.3390/mi14030553.

[17] H. Sariri, Z. Rahmani, A. Lalbakhsh, and S. Majidifar, "Compact LPF using T-shaped resonator", *Frequenz*., Vol. 67, pp. 17–20, 2013.

[18] Z. Wang and C. W. Park, "Multiband pi-shaped structure with resonators for tri-band Wilkinson power divider and tri-band rat-race coupler", In: *Proc of the 2012 IEEE/MTT-S International Microwave Symposium Digest*, Montreal, QC, Canada, pp. 1–3, 2012.

[19] K. Dehghani, G. Karimi, A. Lalbakhsh, and S. V. Maki, "Design of lowpass filter using novel stepped impedance resonator", *Electron. Lett*., Vol. 50, pp. 37–39, 2014.

[20] Q. Zhang, G. Zhang, Z. Liu, W. Chen, and W. Tang, "Dual-band filtering power divider based on a single circular patch resonator with

improved bandwidths and good isolation", *IEEE Trans. Circuits Syst. II Express Briefs*, Vol. 68, pp. 3411–3415, 2021.
[21] S. Chen, S. Qi, X. Chen, G. Sun, and W. Wu, "Five-way radial filtering power divider using back-to-back quarter-mode substrateintegrated waveguide and microstrip resonator", *Electron. Lett*., Vol. 57, pp. 888–890, 2021.
[22] H. A. Hussein, Y. S. Mezaal, and B. M. Alameri, "Miniaturized microstrip diplexer based on fr4 substrate for wireless communications", *Elektronika Ir Elektrotechnika*, Vol. 27, No. 5, pp. 34-40, 2021.
[23] C. F. Chen, K. W. Zhou, R. Y. Chen, H. Y. Tseng, Y. H. He, W. J. Li, and J. H. Weng, "Design of microstrip multifunction integrated diplexers with frequency division, frequency selection, and power division functions", *IEEE Access*. Vol. 9, pp. 53232-53242, 2021.
[24] S. I. Yahya, A. Rezaei, and L. Nouri, "Compact wide stopband microstrip diplexer with flat channels for WiMAX and wireless applications", *IET Circuits, Devices and Systems*, Vol. 14, No. 6, pp. 846-852, 2020.
[25] M. Tahmasbi, F. Razaghian, and S. Roshani, "Design of bandpass-bandpass diplexers using rectangular-, T-, and Lshaped resonators for hybrid power amplifier and 5G applications", *Analog Integrated Circuits and Signal Processing*, Vol. 109, No. 3, pp. 585-597, 2021.
[26] Z. L. Su, B. W. Xu, S. Y. Zheng, H. W. Liu, and Y. L. Long, "High-isolation and Wide-stopband SIW diplexer using mixed electric and magnetic coupling", *IEEE Transactions on Circuits and Systems II: Express Briefs*, Vol. 67, No. 1, pp. 32-36, 2020.
[27] M. Tahmasbi, F. Razaghian, and S. Roshani, "Design of bandpass-bandpass diplexers using rectangular-, T-, and Lshaped resonators for hybrid power amplifier and 5G applications", *Analog Integrated Circuits and Signal Processing*, Vol. 109, No. 3, pp. 585-597, 2021.
[28] A. A. Chinig, L. Errkik, A. E. Abdellaoui, and A. Tajmouati, "Design of a Microstrip Diplexer and Triplexer Using Open Loop Resonators", *Journal of Microwaves, Optoelectronics and Electromagnetic Applications*, Vol. 15, No. 2, 2016, doi: 10.1590/2179-10742016v15i2602.
[29] J. S. Hong, *Microstrip Filters for RF/Microwave Application*, 2nd Edition, Wiley, New York, 2011.
[30] P. Jarry and J. Beneat, *Design and Realizations of Miniaturized Fractal RF and Microwave filter*, A John Wiley & Sons, Inc., Publication, 2009.
[31] A. H. Hussien, H. H. Abdullah, and M. A. Attia, "S-band compact microstrip full duplex Tx/Rx patch antenna with high isolation", *IEEE Antennas and Wireless Propagation Letters*, Vol. 12, No. 10, pp. 2090–2094, 2019, doi: 10.1109/LAWP.2019.2937769.